Quaternary Science Reviews 231 (2020) 106202

Contents lists available at ScienceDirect

Quaternary Science Reviews

journal homepage: www.elsevier.com/locate/quascirev

Wetland expansion on the continental shelf of the northern South China Sea during deglacial sea level rise

Yunru Chen [a, 1], Enqing Huang [a, *, 1], Enno Schefuß [b], Mahyar Mohtadi [b], Stephan Steinke [c], Jingjing Liu [a], Gema Martínez-Méndez [d], Jun Tian [a]

[a] State Key Laboratory of Marine Geology, Tongji University, 200092, Shanghai, China
[b] MARUM - Center for Marine Environmental Sciences, University of Bremen, 28359, Bremen, Germany
[c] Department of Geological Oceanography and State Key Laboratory of Marine Environmental Science, Xiamen University, Xiamen, China
[d] Alfred Wegener Institute, Helmholtz Centre for Polar and Marine Research, Am Alten Hafen 26, 27568, Bremerhaven, Germany

ARTICLE INFO

Article history:
Received 26 September 2019
Received in revised form
28 January 2020
Accepted 28 January 2020
Available online 4 February 2020

Keywords:
Vegetation composition
Plant-wax lipids
Compound-specific carbon isotopes
East Asian monsoon
Coastal environments

ABSTRACT

To identify environmental causes for past changes in vegetation in subtropical East Asia, we present carbon isotope compositions of plant-wax *n*-alkanes and provide estimates of the C_4-plant contribution across the past four glacial terminations and interglacials, based on cores recovered from the northern South China Sea. Our results show a comparable C_4-plant contribution between the Last Glacial Maximum (LGM) and the Holocene. An increase of the C_4-plant contribution by 15–20% is found for Terminations IV, II and I relative to subsequent interglacial peaks, coeval with an expansion of Cyperaceae and Poaceae. In contrast, Termination V reveals a lower C_4-plant contribution than Marine Isotope Stage (MIS) 11c. The data exhibit a long-term trend, with a stepwise increase of the C_4-plant contribution across interglacials MIS 11c, 9e, 7e and 1. We suggest that no substantial changes in humidity levels over glacial-interglacial cycles occurred facilitating a similar C_3/C_4-plant ratio for the LGM and the Holocene. Instead, deglacial sea-level rises caused an extensive development of floodplains and wetlands on the exposed continental shelf, providing habitats for the spread of C_4 sedges and grasses. The progressive subsidence of Chinese coastal areas and the broadening of the continental shelf over the late Quaternary explains the nearly absence of C_4 plant occurrence during Termination V and a gradual increase of the C_4-plant contribution across interglacial peaks. Taken together, changes in coastal environments should be considered when interpreting marine-based vegetation reconstructions from subtropical Asia.

1. Introduction

Monsoon-driven hydroclimate change is a defining feature of low-latitude climatology (Wang et al., 2014). Thus, past changes in tropical-subtropical vegetation composition on tectonic to millennial time scales are usually interpreted in the context of hydroclimate changes. However, in addition to humidity levels, vegetation composition can respond to a variety of other causes including air temperatures, sunlight intensity, soil types, landforms, nutrient status and atmospheric CO_2 concentrations (e.g., Sage, 2004; Bromham and Bennett, 2014). In coastal regions, the transformation of environments during sea-level transgressions can also exert a strong impact on the vegetation (e.g., González and Dupont, 2009; Horton et al., 2018). Therefore, attributing alterations of vegetation types to monsoon dynamics alone can sometimes result in misleading interpretations, which seems to be the case for current paleovegetation studies in subtropical Asia. Vegetation reconstructions derived from terrestrial and marine archives give conflicting results on the evolution of the East Asian summer monsoon over glacial-interglacial cycles (e.g., Sun et al., 2000; Liu and Wang, 2004).

Several palynological reconstructions from lakes and peatlands suggest that southern China and central-southern Taiwan were covered by warm temperate evergreen-deciduous forests with a moderate expansion of herbaceous plants during the Last Glacial Maximum (LGM, 23–19 ka BP) (Liew et al., 2006; Lee and Liew, 2010; Ni et al., 2010; Xiao et al., 2018). This was followed by an expansion of subtropical forests during the last deglaciation, the

* Corresponding author. State Key Laboratory of Marine Geology, Tongji University, 1239 Siping Road, 200092, Shanghai, China.
E-mail address: ehuang@tongji.edu.cn (E. Huang).
[1] Y.C. and E.H. contributed equally to this study.

https://doi.org/10.1016/j.quascirev.2020.106202
0277-3791/

appearance of tropical evergreen broadleaved forests during the early Holocene, and a prevalence of subtropical-tropical forests during the mid-to-late Holocene in southernmost China and southern Taiwan (Lee and Liew, 2010; Ni et al., 2010; Xue et al., 2015; Sheng et al., 2017). An increase in the abundance of subtropical-tropical forests is considered to have been induced by rising air temperatures, and possibly also by elevated humidity levels (Ni et al., 2010; Xue et al., 2015; Sheng et al., 2017). Because southern China and southern Taiwan were not covered by grasslands during the last glacial period, it is believed that monsoonal moisture supply to the subtropical East Asia did not experience substantial changes over glacial-interglacial cycles (Lee and Liew, 2010; Ni et al., 2010).

Marine-based palynological reconstructions from the northeastern South China Sea (SCS, Fig. 1), on the other hand, provide a different view on regional environmental changes (Sun and Li, 1999; Sun et al., 2000, 2003; Luo et al., 2005; Yu et al., 2017). The SCS is surrounded by an extensive continental shelf, which was a large continental area drained by river systems during the LGM due to a sea-level fall of ~120 m relative to today. Therefore, glacial and early deglacial pollen records derived from marine sediment cores contain important information about the vegetational composition on the exposed continental shelf (Sun et al., 2000; Zheng et al., 2013). Available pollen records from five sites of the northeastern SCS reveal that the last two glacial maxima were characterized by a high abundance of herbaceous plants consisting mainly of *Artemisia* and Poaceae (Fig. 1; Sun and Li, 1999; Sun et al., 2000, 2003; Luo et al., 2005; Chang et al., 2013; Dai and Weng, 2015; Yu et al., 2017). These findings were taken as evidence to infer that the exposed continental shelf of the northeastern SCS was covered by grasslands with only sparse subtropical trees during the last two glacial maxima, indicating a substantial weakening of the East Asian summer monsoon and more arid conditions (Sun et al., 2000, 2003; Luo et al., 2005; Yu et al., 2017). This climatic interpretation thus appears in conflict with that derived from southern China and central-southern Taiwan pollen reconstructions as stated above (Liew et al., 2006; Lee and Liew, 2010; Ni et al., 2010; Sheng et al., 2017; Xiao et al., 2018).

Recently, a new marine-based palynological record was obtained from the northwestern SCS (GeoB16602, Fig. 1), which shows similar glacial-to-Holocene changes in pollen assemblage as terrestrial-based reconstructions but differs from the northeastern SCS results, with a modest expansion of herbaceous plants and the absence of *Artemisia* during the LGM (Cheng et al., 2018). Not only does this new pollen record reveal a strong heterogeneity of the glacial vegetation on continental shelf of the northern SCS, it also suggests that the interpretation of marine-based vegetation reconstructions in the context of monsoon changes is probably inappropriate. Therefore, it is necessary to re-evaluate major environmental causes for vegetation changes on the continental shelf of the SCS.

In this study, we provide additional information about vegetational changes on the exposed continental shelf of the northwestern SCS and the surrounding landmass by using plant-wax $\delta^{13}C$ ($\delta^{13}C_{wax}$) reconstructions from marine sediment cores at site GeoB16602 (Fig. 1). In general, $\delta^{13}C_{wax}$ can be used to estimate the relative proportion of C_4 to C_3 plants in terrestrial ecosystem (Farquhar et al., 1989; Collister et al., 1994). We find a moderate expansion of C_4 plants over the recent three glacial terminations, corresponding to an increase in the abundance of Cyperaceae and Poaceae. We further ascribe the C_4-plant expansion to the extensive development of floodplains and wetlands on the continental shelf during deglacial sea-level rise, rather than to changes in East Asian monsoon rainfall.

2. Regional setting

Today, annual mean air temperatures between 20 and 23 °C and high annual rainfall amounts between 1000 and 2300 mm characterize most areas of southern China and Taiwan (19-24°N, Peng et al., 2010; International Atomic Energy Agency, 2013). The region also features a strong precipitation seasonality, generally with

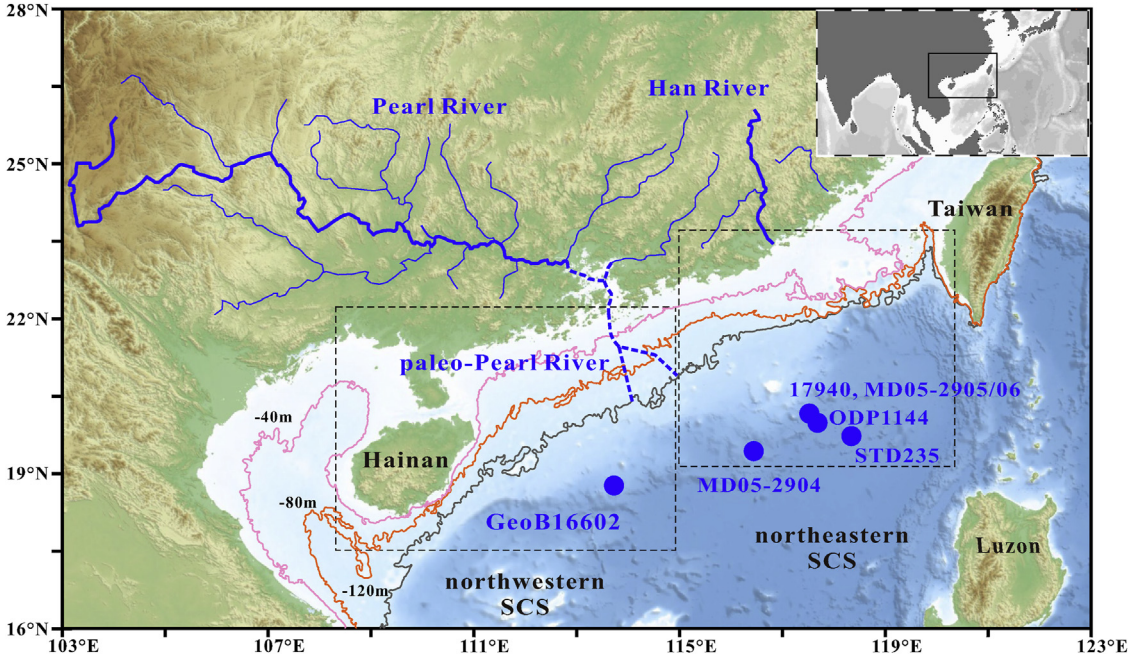

Fig. 1. Regional setting and geographic locations of marine coring sites mentioned in this study. Modern (blue solid lines) and paleo (blue dashed lines) river systems draining southern China. The −120 m, −80 m and −40 m isobath lines and the exposed continental shelves during the LGM are indicated. The area of northwestern and northeastern SCS is indicated by rectangles. (For interpretation of the references to colour in this figure legend, the reader is referred to the Web version of this article.)

~4–10 times more precipitation during summer (May–August) than during winter (November–February). However, winter seasons still receive a total rainfall amount of >150 mm (Peng et al., 2010; International Atomic Energy Agency, 2013), speaking against a clear dry season. Most areas of modern southern China and Taiwan are occupied by subtropical evergreen broadleaved forests due to the high moisture availability, which remained to be covered by warm temperate forests during the last glacial period based on pollen reconstructions (Liew et al., 2006; Lee and Liew, 2010; Ni et al., 2010). Leaf growth and flush is inferred to occur almost year-round in such forests and under such climate conditions (Jackson, 1978; Portmann et al., 2010; Thomas et al., 2014).

In modern southern China and Taiwan, C_3 plants include trees, shrubs and grasses (Bi et al., 2005). C_4 species numbers only occupy ~2.5% of the total species numbers in regional flora, which primarily belong to Poaceae (grasses, ~56% of the total C_4 species numbers) and Cyperaceae (sedges, ~33% of the total C_4 species numbers) (Wang and Ma, 2016). C_4 species of Poaceae and Cyperaceae both increase in number with increasing annual-mean air temperatures and rainfall (Yin and Li, 1997; Wang and Ma, 2016). C_4 species of Chenopodiaceae can only be found in northern and northwestern China under semi-arid/arid climate conditions (Yin and Li, 1997; Wang and Ma, 2016). A compilation of geological reconstructions suggests that the C_4-plant abundance in northern and southern China showed a different sensitivity to climate factors throughout the last glacial-interglacial cycle, with the increased C_4-plant abundance in response to rising temperatures and rainfall in northern China, but the decreased abundance in response to the enhanced rainfall in southern China (Jiang et al., 2019).

Terrigenous input to the northern SCS is predominantly from river systems draining the surrounding landmass and islands, while the contribution of aeolian dust from distant areas is negligible (Liu et al., 2016). At site GeoB16602, fluvial sediment discharge is mainly comprised of material from southern China (the Pearl River, Fig. 1) and southern Taiwan, with a minor contribution from Luzon (Liu et al., 2017; Huang et al., 2018). During the LGM, a total land area of ~$3.9*10^5$ km^2 emerged in the northern SCS, and coastlines extended seaward by ~200 km (Fig. 1). Site GeoB16602 thereby received more sediments from southern China with respect to the Holocene due to the extension of the Pearl River system flowing across the exposed continental shelf (Fig. 1; Liu et al., 2017).

3. Material and methods

3.1. Core material and age model

Sediment cores at site GeoB16602 (18.95°N, 113.71°E, water depth, 953 m) were recovered during the R/V SONNE Cruise SO-221 in 2012 (Mohtadi et al., 2012, Fig. 1). Details regarding the establishment of the composite record and the chronology are described in Huang et al. (2018). Briefly, the age model of the uppermost 5.62 m of the composite record GeoB16602 was constrained by 15 planktonic foraminiferal ^{14}C ages (Fig. 2a, Liu et al., 2017). The chronology of the lower part was established by aligning the benthic foraminiferal $\delta^{18}O$ record between 8.66 and 49.04 m to the reference $\delta^{18}O$ of ODP Site 1146 (Caballero-Gill et al., 2012), and that between 51.44 and 82.72 m to the global benthic $\delta^{18}O$ stack LR04 (Fig. 2a, Lisiecki and Raymo, 2005). The entire sediment sequence covers the period since Marine Isotope Stage (MIS) 13.

3.2. Measurement of molecular biomarkers

A total of 183 samples has been obtained from Termination V-MIS 11, Termination IV-MIS 9, Termination II-MIS 5 and the last glacial-interglacial cycle (Fig. 2). The biomarker analyses were performed at MARUM, University of Bremen, and the entire protocol was described in Huang et al. (2018). In brief, the total lipid extracts of freeze-dried samples (10–15 g for each) were obtained by Accelerated Solvent Extraction and further separated into hydrocarbon, ketone and polar fractions using silica-gel column chromatography. After removal of unsaturated compounds on $AgNO_3$-impregnated Si-columns by elution with hexane, the saturated hydrocarbon fractions were measured on a ThermoFisher Scientific Focus gas chromatograph equipped with a flame ionization detector. Individual *n*-alkanes (*n*-C_{25} to *n*-C_{33} alkanes) were quantified by the integration of chromatogram peak areas calibrated against external standard solutions containing 16 *n*-alkanes and the internal squalene standard. Replicate external standard analyses result in a quantification error of <5%.

Measurements of compound-specific stable carbon isotopes of *n*-C_{29} and *n*-C_{31} alkanes were performed on a Thermo-Fisher Scientific Trace gas chromatograph coupled via a combustion reactor to a MAT 252 mass spectrometer at MARUM, University of Bremen. Carbon isotope values were calibrated against CO_2 reference gas with known isotopic composition and reported as $\delta^{13}C$ in per mil (‰) relative to Vienna Pee Dee Belemnite (VPDB). Standard deviation in 153 samples with duplicate or triplicate measurements is ±0.4‰ and ±0.2‰ for *n*-C_{29} and *n*-C_{31} alkane $\delta^{13}C$, respectively. Measurements of the squalene internal standard yielded a precision and an accuracy of 0.4‰ and <0.1‰ (n = 346), respectively. External *n*-alkane standards with known isotopic compositions were run after every sixth sample. The long-term mean absolute deviation of the external standards was <0.2‰.

3.3. Estimating the relative contribution of C_4 plants

$\delta^{13}C_{wax}$ values are determined by a set of factors including the $\delta^{13}C$ of atmospheric CO_2, fractionation against ^{13}C during photosynthesis and lipid biosynthesis, and changes in ^{13}C fractionation induced by climate changes (Farquhar et al., 1989; Collister et al., 1994; Diefendorf and Freimuth, 2017). Changes in $\delta^{13}C$ values of atmospheric CO_2 are less than 0.6‰ over the past 150 thousand years (Schmitt et al., 2012; Eggleston et al., 2016), without considering the most recent 150 years when the global carbon cycle is severally perturbated by human activities (the Suess effect). Thereby, changing $\delta^{13}C$ values of atmospheric CO_2 are a minor issue when interpreting $\delta^{13}C_{wax}$ variations over the late Quaternary. Plants using different photosynthetic pathways can synthesize wax lipids with distinct $\delta^{13}C$ compositions, with a generally larger depletion of ~15‰ in C_3 plants compared to C_4 plants (Diefendorf and Freimuth, 2017). ^{13}C fractionation associated with lipid biosynthesis is currently impossible to quantify, because data for different plant communities are still sparse and scattered (Diefendorf and Freimuth, 2017). In the East Asian monsoonal region, water availability and temperature are estimated to affect $\delta^{13}C_{wax}$ values by less than ~0.6‰, respectively, over glacial-interglacial cycles, and these two effects tend to cancel out each other (Yang et al., 2015). Taken together, C_3/C_4 carbon fixation pathways generate the largest difference in $\delta^{13}C_{wax}$ values.

$\delta^{13}C_{wax}$ signals can be well retained during transport and after burial in sediments, because of chemical inertness of plant waxes (Diefendorf and Freimuth, 2017 and references therein). Therefore, sedimentary $\delta^{13}C_{wax}$ is generally accepted as a proxy to disentangle contributions by C_3 and C_4 plants. Furthermore, the C_3/C_4-plant contributions can provide implications on the relative abundance of C_3/C_4 plants in the terrestrial ecosystem, although plants produce very different amounts of waxes (Diefendorf and Freimuth, 2017).

Modern investigations in subtropical-tropical East Asia reveal a mean *n*-C_{31} alkane $\delta^{13}C$ value of -35.2 ± 2.6‰ ($\pm 1\sigma$ standard error,

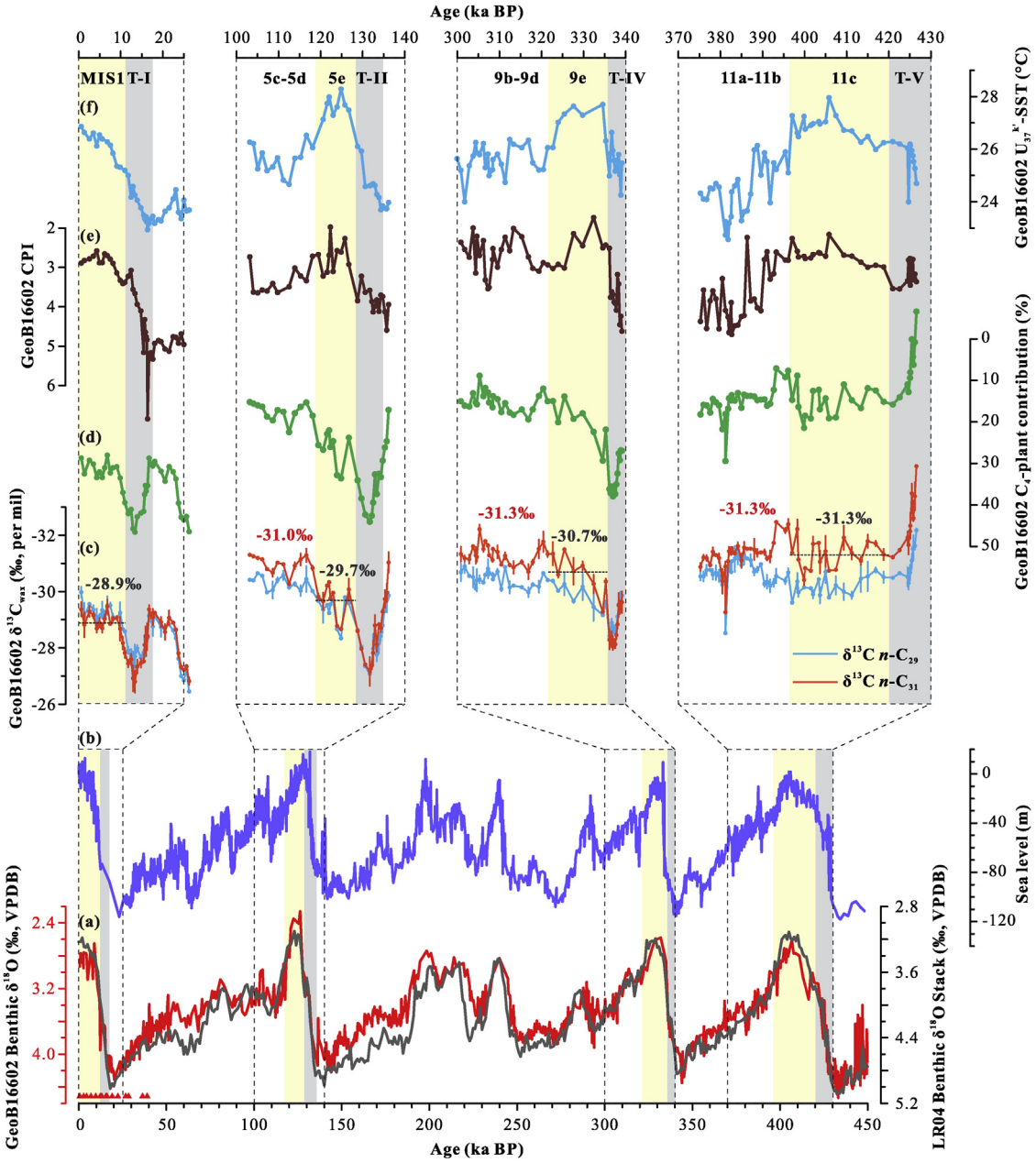

Fig. 2. Age model and biomarker records of site GeoB16602. (a) Site GeoB16602 benthic $\delta^{18}O$ (red, Huang et al., 2018) and global benthic $\delta^{18}O$ stack of LR04 (grey, Lisiecki and Raymo, 2005). The visual alignment of both records was used to establish the age model with the addition of AMS ^{14}C dates (triangles, Liu et al., 2017) in the upper part of the record. (b) Sea-level reconstructions from the Red Sea (Grant et al., 2014). (c) $\delta^{13}C$ of *n*-C_{29} and *n*-C_{31} alkanes associated with ±1σ standard errors. Average values of *n*-C_{31} $\delta^{13}C$ for each interglacial peak and sub-interglacial are denoted. (d) Estimates of the C_4-plant contribution. (e) Carbon-number preference index ($CPI_{25\text{-}33}$) (Huang et al., 2018). (f) *UK′* 37-SST (Huang et al., 2018). The duration of interglacial peaks and glacial terminations are indicated by yellow and grey bars, respectively. (For interpretation of the references to colour in this figure legend, the reader is referred to the Web version of this article.)

n = 43) and −20.8 ± 2.4‰ (±1σ standard error, n = 14) for C_3 and C_4 plants, respectively (Chikaraishi and Naraoka, 2003; Bi et al., 2005; Jia et al., 2015). These two end-member values were adjusted by +1.7‰ in order to account for the difference in the $\delta^{13}C$ of atmospheric CO_2 between the present and the Preindustrial Era (the Suess effect, Mauna Loa Observatory, ftp://aftp.cmdl.noaa.gov; Schmitt et al., 2012). The adjusted end-member values and a binary mixing equation were applied to provide estimates of the relative C_3/C_4 plant contributions in the past:

$$\text{Measured } n-C_{31}\,\delta^{13}C = (100\% - x) * -33.50 + x * -19.1‰,$$

where x indicates the relative contribution by C_4 plants.

Considering uncertainties associated with $\delta^{13}C$ measurements and end-member values, the mean propagated error for the estimates of the C_4-plant contribution is as large as ±15% (±1σ standard error). It should be noted that modern $\delta^{13}C_{wax}$ end-member values of C_3 and C_4 plants are not well defined in the literature and can vary through time due to changes in vegetation types, climate conditions and $\delta^{13}C$ of atmospheric CO_2. These factors explain the large errors of estimates. In natural ecosystems, however, the end-member values are expected to be much better defined which should result in lower error estimates. Nevertheless, we provide these estimates to give an idea to what extent the terrestrial

ecosystem in the source area changed over time.

Along with $\delta^{13}C_{wax}$ results, other proxy records of site GeoB16602 are also presented in this study. Results of the carbon-number preference index (CPI_{25-33}), *UK′* 37-sea surface temperatures (*UK′* 37-SST) and stable hydrogen isotope values of *n*-alkanes (δD_{wax}) at this site have been published by Huang et al. (2018), and foraminiferal Mg/Ca-SST as well as pollen assemblage data have been presented in Cheng et al. (2018).

4. Results

The *n*-alkane chain lengths range from C_{21} to C_{33}, with *n*-C_{29} and *n*-C_{31} being the most abundant alkanes. The CPI_{25-33} varies between 2.0 and 5.0 with a mean value of 3.4, revealing a pronounced glacial-interglacial cyclicity (Fig. 2e). In general, the CPI_{25-33} has relatively high values during glacial Terminations IV, II and I as well as the last glacial, and low values during peak interglacials MIS 11c, 9e, 5e and 1.

Carbon isotope values of the *n*-C_{31} alkane show consistent variations with the *n*-C_{29} alkane ($n = 179$, $r = 0.94$, $p < 0.001$) but with more pronounced changes over the four time intervals investigated in this study (Fig. 2c). The *n*-C_{31} $\delta^{13}C$ values range from −34.5‰ to −26.8‰, and the estimated C_4-plant contribution changes between 0 and 46%. Both do not vary in concert with glacial cycles but show several distinct features. First, during the LGM and the latest part of MIS 6, *n*-C_{31} $\delta^{13}C$ values are comparable to those during the Holocene and MIS 5e, respectively. Second, over Terminations IV, II and I, the *n*-C_{31} $\delta^{13}C$ record shows a three-phase change, a rapid initial increase is followed by rather constant (enriched) values that ultimately decrease to the interglacial-peak level. This corresponds to an increase of 15–20% in the C_4-plant contribution during the early phases of glacial terminations. In contrast, *n*-C_{31} $\delta^{13}C$ values over Termination V show a rapid increase from a very depleted level of −34.5‰ to −32.0‰, and then remain at similar levels as those during the subsequent interglacial. Third, *n*-C_{31} $\delta^{13}C$ values during MIS 9d-9b and 5d-5c are more depleted than during MIS 9e and 5e, respectively. Finally, the comparison of different interglacial peaks shows a stepwise enrichment of *n*-C_{31} $\delta^{13}C$ values over MIS 11c, 9e, 5e and 1, with mean values of −31.3‰, −30.7‰, −29.7‰ and −28.9‰, respectively.

5. Discussion

5.1. Source of plant waxes

At site GeoB16602, the CPI_{25-33} is above 2 during all four investigated periods (Fig. 2e), indicative of an odd-over-even carbon-number predominance, and thus a major terrestrial higher plant origin of the *n*-alkanes (Eglinton and Hamilton, 1967). The close correlation between the CPI values and sea level over glacial-interglacial cycles is a common feature found in northern SCS sedimentary records (He et al., 2008; Zhou et al., 2012). Compared to interglacial periods, the shorter distance between the coastlines and coring sites during glacials, combined with lower temperatures, decreased degradation and microbial alteration of terrestrial *n*-alkanes during soil storage and land-to-ocean transport. This explains the presence of relatively high and low CPI values during glacial-deglacial and interglacial periods, respectively, at site GeoB16602.

Another aspect which deserves attention before discussing glacial-interglacial $\delta^{13}C_{wax}$ variations in terms of vegetation changes, is the flooding of the continental shelf (Fig. 1). Soil remobilization could have resulted in a transfer of reworked sediments from the shelf to the slope and deep basins during sea level rise. However, deglacial $\delta^{13}C_{wax}$ values at site GeoB16602 are rather different from those of glacial maxima (Fig. 2c), implying that the possible contribution of reworked materials did not substantially overprint the deglacial $\delta^{13}C_{wax}$ signals. Therefore, $\delta^{13}C_{wax}$ reconstructions of site GeoB16602 should largely reflect changes in regional vegetation composition. Especially, site GeoB16602 received fresher *n*-alkanes (i.e. with a high CPI) from the adjacent continental shelf during low sea-level periods than during interglacial periods. For that reason, glacial and deglacial $\delta^{13}C_{wax}$ reconstructions should tend to reflect vegetation changes on the shelf, similar to that of pollen records from the marine realm (Sun et al., 2000; Zheng et al., 2013).

5.2. Comparison of pollen and $\delta^{13}C_{wax}$ from the northern SCS

A comparison of pollen and $\delta^{13}C_{wax}$ reconstructions can help to identify the origin of plant families contributing to changes in C_3/C_4-plant abundances. Pollen records from the northern SCS are usually characterized by very high percentages of *Pinus*, with 60–90% during interglacial and 30–50% during glacial periods (Sun et al., 2000, 2003; Luo et al., 2005; Chang et al., 2013; Yu et al., 2017; Cheng et al., 2018). This is partly because *Pinus* genera have a high productivity of pollen, and *Pinus* pollen have much stronger transport capabilities via ocean currents and wind compared to other pollen taxa due to their low density and airbag structure (Luo et al., 2014; Dai and Weng, 2015; Yu et al., 2017). Therefore, *Pinus* pollen are usually overrepresented in the pollen assemblages of deep-sea sediments from the northern SCS, particularly during interglacial high sea-level periods. For a more reasonable comparison of temporal changes between pollen and $\delta^{13}C_{wax}$ reconstructions, the *Pinus* fraction is thus removed when calculating percentages of other pollen taxa.

At site GeoB16602, pollen of herbaceous plants mostly derive from Cyperaceae and Poaceae (Cheng et al., 2018), among which some genera of Poaceae and most genera of Cyperaceae belong to C_4 plants (Xue et al., 2014). Chenopodiaceae were absent from pollen taxa for the recent several glacial terminations and interglacials (Cheng et al., 2018). As shown in Fig. 3, the *n*-C_{31} $\delta^{13}C$ record of site GeoB16602 broadly matches the pollen records. Especially during Termination IV, II and I, an increase in the relative contribution of C_4 plants by up to 15–20% corresponds to a pronounced increase in %Cyperaceae and %Poaceae. Termination V with very negative *n*-C_{31} $\delta^{13}C$ values is associated with no increase in either %Cyperaceae or %Poaceae. MIS 11c and 9e are characterized by less contributions of C_4 plants than MIS 5e and 1, coincident with lower %Cyperaceae during MIS 11c and 9e than during the latter two interglacial peaks. Pollen and $\delta^{13}C_{wax}$ reconstructions, however, also show disagreements during some periods. For instance, an increase of %Poaceae during the LGM with respect to the Holocene is not reflected in *n*-C_{31} $\delta^{13}C$, indicating that the glacial expansion of Poaceae was mainly due to C_3 grass species.

The relationship between $\delta^{13}C_{wax}$ and pollen, however, is different in cores from the northeastern SCS (Fig. 4). Compared to subsequent interglacial periods, there was a prominent expansion of C_4 plants during the last two glacial maxima and glacial terminations around the northeastern SCS (Zhou et al., 2012; He et al., 2017). In pollen records, %Poaceae is relatively high during the two glacial maxima but not during glacial terminations, while % Cyperaceae largely remains invariant over the last two glacial-interglacial cycles (Fig. 4; Sun et al., 2003; Luo et al., 2005; Dai and Weng, 2015; Dai et al., 2015). This suggests that the glacial expansion of C_4 plants around the northeastern SCS is mainly due to an increase in the abundance of C_4 species of Poaceae. Plant taxa responsible for the deglacial C_4-plants expansion, however, cannot be identified in pollen records from the northeastern SCS.

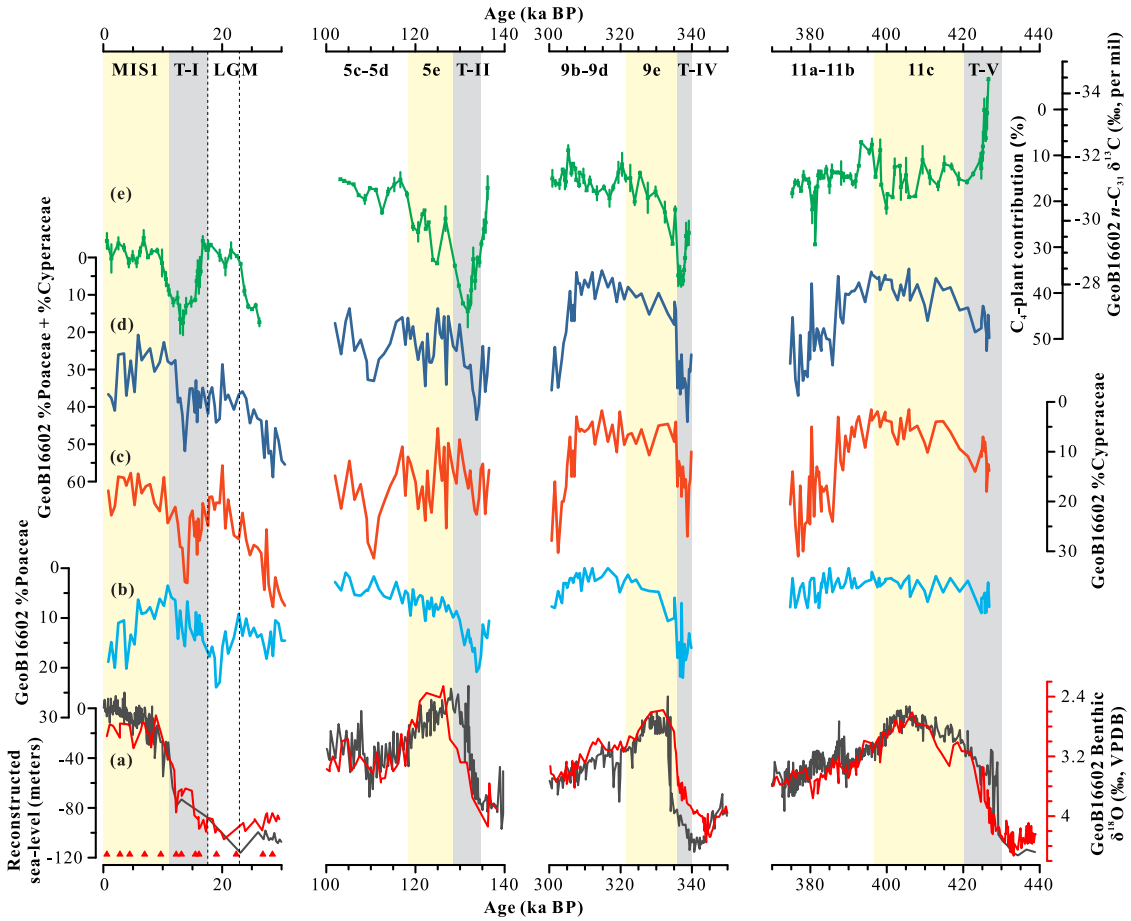

Fig. 3. Comparison of pollen and $\delta^{13}C$ of n-C_{31} alkane reconstructions at site GeoB16602 over four glacial terminations and interglacial periods. (a) Site GeoB16602 benthic $\delta^{18}O$ for stratigraphic control (red, Huang et al., 2018) and sea-level reconstructions from the Red Sea (grey, Grant et al., 2014). Triangles indicate AMS ^{14}C dates. In (b), (c) and (d), the percentage of Poaceae, Cyperaceae, and the sum percentage of these two plant families (Cheng et al., 2018). Note that the *Pinus* fraction is removed when calculating the relative abundance of these plant taxa. (e) The n-C_{31} $\delta^{13}C$ reconstruction with $\pm 1\sigma$ standard errors and estimates of the C_4-plant contribution at Site GeoB16602. The duration of interglacial peaks and glacial terminations are indicated by yellow and grey bars, respectively. (For interpretation of the references to colour in this figure legend, the reader is referred to the Web version of this article.)

5.3. No substantial changes in humidity levels between glacial maxima and interglacial peaks

In general, C_4 grasses (mainly comprising of Poaceae in southern China) can outcompete C_3 relatives in tropical and subtropical areas under low CO_2 levels, high growing-season temperatures, arid and summer-concentrated rainfall conditions (e.g., Ehleringer et al., 1997; Huang et al., 2001; Schefuβ et al., 2003, 2005; Ehleringer, 2005). However, as noted above, C_4 species of Poaceae also tend to grow in wet and warm environments in China (Yin and Li, 1997; Wang and Ma, 2016). The climatic significance of C_4 species of Poaceae in southern China and Taiwan is thus likely different from other monsoonal regions, such as in India where the species number of C_4 grasses (Poaceae) is anti-correlated with annual rainfall amount (Takeda, 1985; Contreras-Rosales et al., 2014). C_4 sedges (Cyperaceae) are important plant types in wetlands in the tropics and subtropics, and are therefore indicators of relatively humid conditions in specific environments (e.g., Yin and Li, 1997; Wang and Ma, 2016; Caley et al., 2018).

With respect to the Holocene, the LGM annual-mean surface temperature was only 4–6 °C cooler in southern China (Fig. 2f; Chu et al., 2017; Cheng et al., 2018; Huang et al., 2018), which is well above the threshold temperature for the growth of C_4 plants (Yin and Li, 1997; Ehleringer, 2005). A global study suggests that the ~80 ppm difference of atmospheric CO_2 partial pressure between glacial and interglacial periods is not a major cause for alteration of the distribution of C_3/C_4 plants in the tropics and subtropics (e.g., Huang et al., 2001; Schefuβ et al., 2003, 2005; 2011; Contreras-Rosales et al., 2014). Accordingly, we consider that varying humidity levels and changes in coastal environments are more important when interpreting changes in the C_4-plant contribution around the northern SCS.

The glacial monsoonal rainfall intensity over southern China is still uncertain due to the lack of reliable reconstructions. Although Chinese stalagmite $\delta^{18}O$ has been widely cited as an indicator of the East Asian summer monsoon strength, more and more evidence suggests that shifts in Chinese stalagmite $\delta^{18}O$ do not solely reflect monsoon rainfall variations at cave locations in central and southern China (Liu et al., 2014; Huang et al., 2018; Tabor et al., 2018). The δD_{wax} of site GeoB16602 gives no clear hints on regional rainfall changes and shows a poor correlation with n-C_{31} $\delta^{13}C$ results ($n = 159$, $r = 0.15$, $p = 0.06$, Fig. 5, Huang et al., 2018). Precipitation isotope records from subtropical East Asia, derived from stalagmites or plant waxes, are usually subject to influences from a set of factors, including changes in convection intensity over moisture source areas, isotope fractionation along moisture trajectories, mixing ratios of different moisture sources, and rainfall seasonality (Huang et al., 2018; Contreras-Rosales et al., 2019).

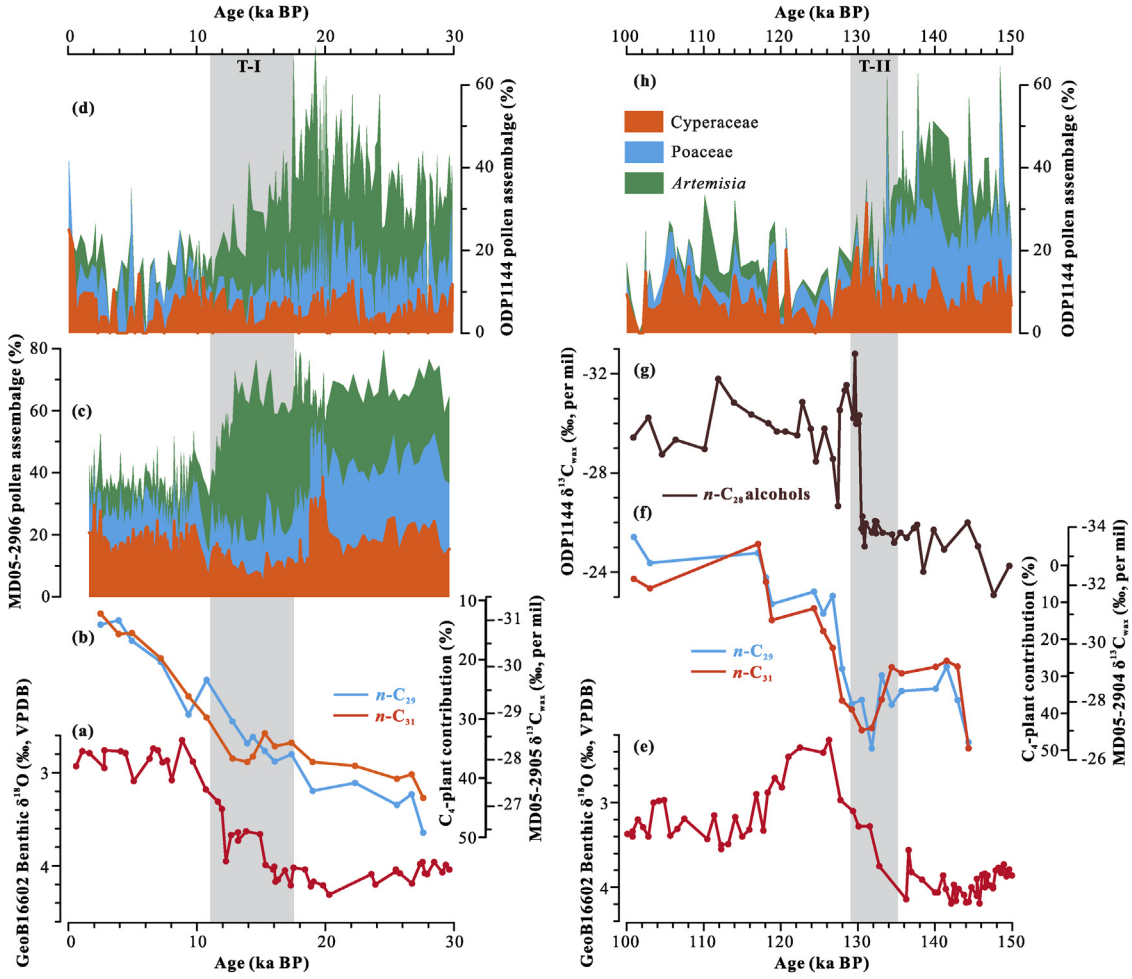

Fig. 4. Comparison of pollen and $\delta^{13}C_{wax}$ reconstructions from the northeastern SCS over the last two glacial-interglacial cycles. In (a) and (e), Site GeoB16602 benthic $\delta^{18}O$ for stratigraphic control (Huang et al., 2018). In (b) and (f), $\delta^{13}C_{wax}$ reconstructions and estimates of the C_4-plant contribution at core MD05-2905 (Zhou et al., 2012) and MD05-2904 (He et al., 2017). (g) The $\delta^{13}C_{wax}$ reconstruction derived from long-chain alcohols at ODP site 1144 (He et al., 2017). In (c), (d) and (h), pollen assemblages from ODP site 1144 (Sun et al., 2003; Luo et al., 2005) and core MD05-2906 (Dai and Weng, 2015; Dai et al., 2015). Note that the *Pinus* fraction is removed when calculating the relative abundance of these plant taxa. The age model of ODP site 1144 has been readjusted to that of ODP site 1146 by visual correlation of planktonic foraminiferal $\delta^{18}O$ (Bühring et al., 2004; Caballero-Gill et al., 2012). Locations of these marine sediment cores are indicated in Fig. 1. The duration of glacial terminations is indicated by grey bars.

These influences can mask the amount effect in precipitation isotope records.

The humidity levels during the LGM over southern China and Taiwan can be inferred from two lines of evidence. First, a compilation of pollen records suggests that the vegetation belt over glacial southern China and central-southern Taiwan was warm temperate forests (Liew et al., 2006; Lee and Liew, 2010; Ni et al., 2010), indicative of sufficient moisture supply to sustain forest vegetation. A majority of $\delta^{13}C_{wax}$ reconstructions from the entire southern China also reveals that the C_4-plant contribution was always below 20% in the interval 22–5 ka BP (Cui et al., 2018). Very few terrestrial records from southern China extend back to earlier glacial periods. One available pollen record suggests that MIS 8 and 6 were wetter than the LGM in the southernmost part of China (Zheng and Lei, 1999). Second, climate simulations imply a mere reduction of ~200 mm/yr in precipitation, and a slight mitigation of precipitation seasonality during the LGM relative to the late Holocene in southern China (Tharammal et al., 2013; Liu et al., 2014). This reduction in glacial rainfall was probably counteracted by a contemporary decrease in potential evapotranspiration due to cooling, which resulted in wetter conditions during the LGM compared to the present (Liu et al., 2018). Taken together, the LGM humidity levels were likely similar to those of today in southern China and Taiwan. This combined with persistently above-threshold temperatures can explain the comparable C_3/C_4 ratio between the LGM and the Holocene, and also between the latest part of MIS 6 and MIS 5e, at site GeoB16602.

In the northeastern SCS, an increase in the glacial abundance of C_4 species of Poaceae with respect to MIS 5e and 1 (Zhou et al., 2012; He et al., 2017), as mentioned above, does not necessarily indicate pronounced moisture changes (Yin and Li, 1997). The northeastern SCS sites are also characterized by a marked increase of *Artemisia* (C_3 grass) during glacial periods compared to MIS 5e and 1 (Fig. 4, Sun et al., 2000, 2003; Luo et al., 2005; Yu et al., 2017; Dai and Weng, 2015), which are of low abundance in terrestrial records from glacial southern China and southern Taiwan (Liew et al., 2006; Ni et al., 2010; Wang et al., 2012; Xue et al., 2015; Sheng et al., 2017) and absent in cores of site GeoB16602 (Cheng et al., 2018). Today, *Artemisia* is a typical plant family abundant in temperate steppes of East Asia (Sun and Li, 1999). However, the presence of high %*Artemisia* in the northeastern SCS cores does not indicate a large southward shift of regional vegetation and a substantial reduction of humidity levels during glacial periods, because southern China was still dominated by warm temperate forests

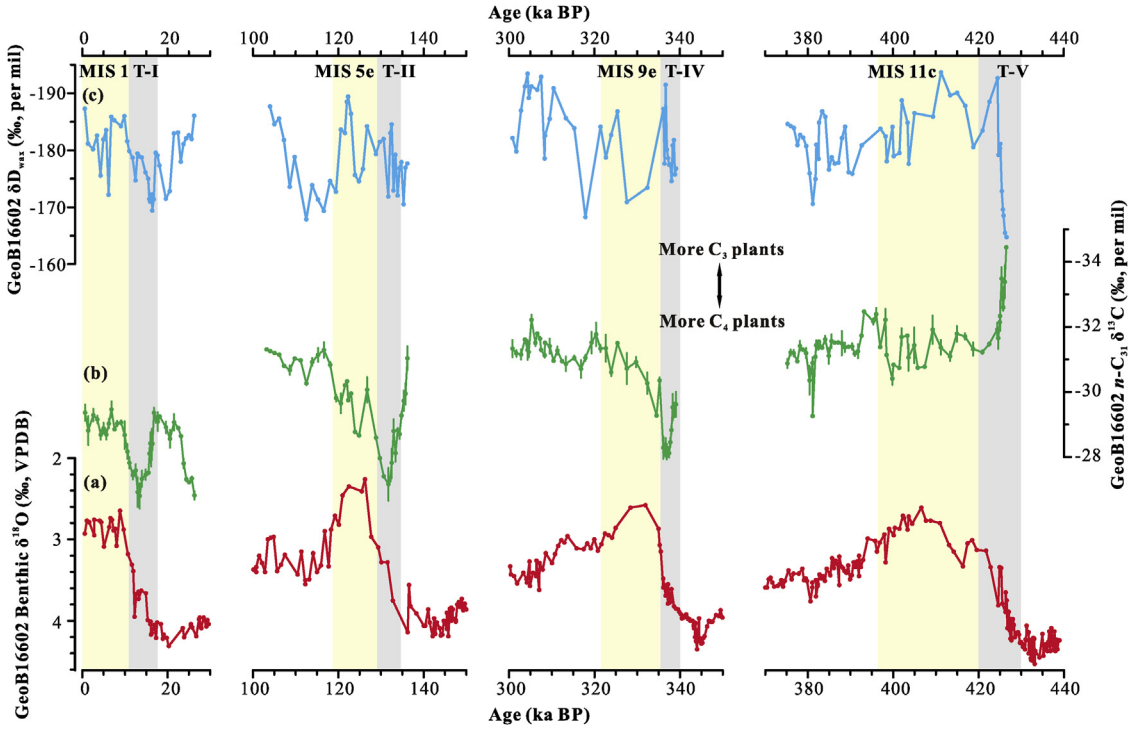

Fig. 5. Comparison of n-C_{31} $\delta^{13}C$ and δD_{wax} records at site GeoB16602 over four glacial terminations and interglacial periods. (a) Site GeoB16602 benthic $\delta^{18}O$ for stratigraphic control (Huang et al., 2018). (b) The n-C_{31} $\delta^{13}C$ reconstruction with ±1σ standard errors. (c) The δD_{wax} reconstruction after adjusted for changes in seawater isotope composition and temperature (Huang et al., 2018). The duration of interglacial peaks and glacial terminations are indicated by yellow and grey bars, respectively. (For interpretation of the references to colour in this figure legend, the reader is referred to the Web version of this article.)

during glacials (Wang et al., 2012; Xue et al., 2015; Sheng et al., 2017). *Artemisia* were thus inferred to grow only in coastal regions of the northeastern continental shelf possible due to their tolerance for salty environments (Liu and Wang, 2004). This has also been the case for the glacial East China Sea, where Cyperaceae, *Artemisia* and Poaceae were found abundant on the flat exposed continent shelf (Zheng et al., 2013).

5.4. Sea-level rise caused the expansion of C_4 plants across glacial terminations

At site GeoB16602, the expansion of C_4 plants during the early phases of glacial Termination IV, II and I is unlikely to be induced by a reduction in humidity with respect to glacial maxima. In contrast, increased abundance of subtropical forest taxa in pollen records from southern China and Taiwan suggests an intensified hydrological cycle during the last deglaciation relative to the LGM (Liew et al., 2006; Ni et al., 2010; Xue et al., 2015; Sheng et al., 2017). In addition, the deglacial C_4-plant contribution was similar to or less than that of the LGM in southern China (Cui et al., 2018), implying that the deglacial C_4-plant expansion at site GeoB16602 was sourced from the exposed continental shelf. Therefore, we infer that coastal environmental changes associated with deglacial sea-level rise (Fig. 3a, Grant et al., 2014) have caused changes in the vegetation composition.

The deglacial flooding of the continental shelf can give rise to the reduction in the hydrologic gradient of river systems, resulting in backlogging of sediments and formation of floodplains (Fig. 6). Combined with the intensified hydrological cycle this likely resulted in the development of extensive wetland environments on the northern SCS continental shelf. C_4 sedges (Cyperaceae) and grasses (Poaceae), which are more competitive species in disturbed habitats and have higher salt tolerance than C_3 plants, are main vegetation types in floodplains, salt marshes and wetlands in the tropics-subtropics (Fig. 6, Sage, 2004; Zheng et al., 2013; Bromham and Bennett, 2014). Therefore, we suggest that the flooding of the exposed continental shelf and the extensive development of floodplains and wetlands are responsible for the deglacial C_4-plant expansion, as inferred from the simultaneous increase in the abundance of Cyperaceae and Poaceae in the pollen records of site GeoB16602 (Fig. 3b and c). This scenario has previously been inferred for the Cariaco Basin in the western tropical Atlantic, where rapid sea-level rise across several Heinrich intervals within MIS 3 caused prominent expansions of salt marsh vegetation (Chenopodiaceae, Poaceae and Cyperaceae) along coastal regions (González and Dupont, 2009). We note that a decrease of the C_4-plant contribution occurred at site GeoB16602 during the latter phase of glacial terminations II and I, when the sea-level rise still continued (Fig. 3b and c). A shrinkage of exposed continent-shelf areas and an already prolonged distance between coastlines and coring sites (Fig. 1) probably resulted in a dilution of shelf-sourced vegetation composition signals at our site, giving rise to the observed reduction of the C_4-plant contribution. This inference is supported by decreased $CPI_{25\text{-}33}$ values during the latter phase of deglaciations (Fig. 2e), which indicates a decreased input of relatively fresh n-alkanes from the shelf to the coring site.

Large-scale subsidence of coastal areas of eastern China and the establishment of a broad continental shelf around China are thought to have occurred progressively over the last several glacial-interglacial cycles, referred to as neotectonics of the Chinese continent (Li, 1991; Li and Fang, 1996). Especially the altitude of coastal areas and the width/size of the continental shelf were inferred to have approached modern values after MIS 6 (Wang et al., 1981, 1985; Sun et al., 2003). Changes in terrigenous input to the northern SCS support this inference. Over the past 350 thousand years, the exposure and the flooding of the continental

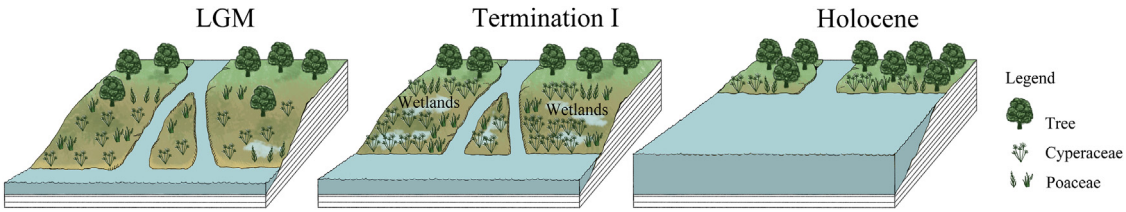

Fig. 6. Schematic representation of the glacial-interglacial evolution of vegetation types around the northwestern SCS. (a) The exposed continental shelf and the flourishing of C_3 plants during the LGM. (b) The deglacial development of wetlands and floodplains on the exposed continental shelf as well as the expansion of Cyperaceae and Poaceae. (c) The drowned continental shelf and the flourishing of subtropical forests during the Holocene.

shelf altered the distance between paleo-coastlines and marine coring locations, resulting in a tight correlation between sea-level changes and terrigenous *n*-alkane abundance as well as the CPI records from the SCS (Fig. 2e, e.g., Pelejero, 2003; He et al., 2008, Huang et al., 2018). However, at site GeoB16602, this does not apply to Termination V. Changes in the CPI values (Fig. 2e) and *n*-alkanes abundance (Huang et al., 2018) do not follow sea-level fluctuations, indicative of a limited shift in paleo-coastlines, at that time. Therefore, the lack of an extensive, low-relief continental shelf during Termination V could have hindered the development of large floodplains and wetlands, unfavorable for the spread of Cyperaceae and Poaceae (Fig. 3b and c). Likewise, a progressive subsidence of southern China as well as an expansion of coastal floodplain areas is capable of explaining the stepwise increase in the C_4-plant contribution across interglacial peaks MIS11c, 9e, 5e and 1 (Fig. 2c and d).

This interpretation does not fit to data from the northeastern SCS, where the deglacial C_4-plant expansion is not associated with an increase in %Cyperaceae and %Poaceae (Fig. 4). Different landform settings on the northwestern and the northeastern SCS continental shelf probably caused this spatial heterogeneity. Due to the prevailing surface currents, the sediment discharge from the paleo-Pearl River system was mainly delivered westward and accumulated along the northwestern SCS continental slope (Liu et al., 2017). The paleo-river systems flowing across the northeastern shelf probably were much smaller than on the western side, given that the runoff and the draining area of the Han River today is an order of magnitude smaller than those of the Pearl River (Fig. 1, Milliman and Farnsworth, 2011). A large fraction of terrigenous sediments in the northeastern SCS is also sourced from Taiwan (Fig. 1, Liu. et al., 2016; Liu et al., 2017). Mountainous rivers on Taiwan show massive sediment discharge but have very small drainage areas and runoff (Milliman and Farnsworth, 2011). The development of floodplains and wetlands, which are usually associated with extended river systems, should therefore have been limited on the northeastern continental shelf. This might have further limited the expansion of Cyperaceae and Poaceae. The inferred landforms on the drowned northern SCS continental shelf, however, are impossible to assess by seismic survey data and sedimentary records. This is because deglacial sea-level rises washed away fine-grained sediments, with only relict sand present in most areas of the modern northern shelf (Liu et al., 2009).

6. Conclusions

$\delta^{13}C_{wax}$ records from site GeoB16602, together with an increasing number of palynological reconstructions from terrestrial and marine archives of southern China, Taiwan and the SCS, allow identifying mechanisms for vegetation changes in subtropical Asia. Glacial temperatures did not fall below the threshold value for the growth of C_4 plants. Combined with modest changes in glacial humidity with respect to the late Holocene, this resulted in a comparable C_4-plant contribution during the LGM and the Holocene on the exposed continental shelf of the northwestern SCS and in southern China.

In the northwestern SCS, deglacial sea-level rise and the subsequent flooding of the flat continental shelf resulted in the establishment of floodplain and wetland environments. Flourishing of Cyperaceae and Poaceae in these environments led to the expansion of C_4 plants during Terminations IV, II and I, as found at site GeoB16602. In contrast, the lack of a broad and low-relief continental shelf during Termination V can explain the nearly absence of C_4 plants at that time. The gradual subsidence of Chinese coastal areas and the progressive expansion of coastal floodplain areas resulted in a stepwise increase of the C_4-plants contribution across interglacial peaks MIS 11c, 9e, 5e and 1. In the northeastern SCS, the lack of large river systems flowing across the exposed shelf might have suppressed the development of floodplains and wetlands during glacial terminations, which limited the expansion of Cyperaceae and Poaceae. We conclude that changes in coastal environments on the exposed continental shelf were an important cause for differences between marine- and terrestrial-based vegetation reconstructions and the spatial heterogeneity of the distribution of vegetation types.

Acknowledgements

We thank the crew and the scientific party of RV Sonne cruise SO-221, R. Kreutz for the assistance in the organic geochemical laboratory, Z. Cheng for discussions and reviewers for constructive comments. E.H. is funded by the NSFC (41776054, 41525020) and the National Key Research and Development Program (2018YFE0202400). The isotope analyses were supported by the DFG-Research Center/Cluster of Excellence, "The Ocean in the Earth System" at MARUM - Center for Marine Environmental Sciences. This project is also funded by the German BMBF grants CARIMA (03G0806B) and INVERS (03G0221A).

Appendix A. Supplementary data

Supplementary data to this article can be found online at https://doi.org/10.1016/j.quascirev.2020.106202.

References

Bi, X.H., Sheng, G.Y., Liu, X.H., Li, C., Fu, J.M., 2005. Molecular and carbon and hydrogen isotopic composition of *n*-alkanes in plant leaf waxes. Org. Geochem. 36, 1405–1417.

Bromham, L., Bennett, T.H., 2014. Salt tolerance evolves more frequently in C_4 grass lineages. J. Evol. Biol. 27, 653–659.

Bühring, C., Sarnthein, M., Erlenkeuser, H., 2004. Toward a high-resolution isotope stratigraphy of the last 1.1 million years: site 1144, South China Sea. In: Prell, W.L., Wang, P., Blum, P., et al. (Eds.), Proc. ODP, Sci. Results, vol. 184, pp. 1–29 (online).

Caballero-Gill, R.P., Clemens, S.C., Prell, W.L., 2012. Direct correlation of Chinese speleothem $\delta^{18}O$ and South China Sea planktonic $\delta^{18}O$: transferring a speleothem chronology to the benthic marine chronology. Paleoceanography 27,

PA2203. https://doi.org/10.1029/2011PA002268.
Caley, T., Extier, T., Collins, J.A., Schefuß, E., Dupont, L., Malaizé, B., Rossignol, L., Souron, A., McClymont, E.L., Jimenez-Espejo, F.J., García-Comas, C., Eynaud, F., Martinez, P., Roche, D.M., Jorry, S.J., Charlier, K., Wary, M., Gourves, P.-Y., Billy, I., Giraudeau, J., 2018. A two-million-year-long hydroclimatic context for hominin evolution in southeastern Africa. Nature 560, 76–79.
Chang, L., Luo, Y., Sun, X., 2013. Paleoenvironmental change based on a pollen record from deep sea core MD05-2904 from the northern South China Sea during the past 20000 years. Chin. Sci. Bull. 58, 3079–3087.
Cheng, Z., Weng, C., Steinke, S., Mohtadi, M., 2018. Anthropogenic modification of vegetated landscapes in southern China from 6,000 years ago. Nat. Geosci. 11, 939–943.
Chikaraishi, Y., Naraoka, H., 2003. Compound-specific δD-δ^{13}C analyses of n-alkanes extracted from terrestrial and aquatic plants. Phytochemistry 63, 361–371.
Chu, G., Sun, Q., Zhu, Q., Shan, Y., Shang, W., Ling, Y., Su, Y., Xie, M., Wang, X., Liu, J., 2017. The role of the Asian winter monsoon in the rapid propagation of abrupt climate changes during the last deglaciation. Quat. Sci. Rev. 177, 120–129.
Collister, J.W., Rieley, G., Stern, B., Eglinton, G., Fry, B., 1994. Compound-specific δ^{13}C analyses of leaf lipids from plants with differing carbon dioxide metabolisms. Org. Geochem. 21, 619–627.
Contreras-Rosales, L.A., Jennerjahn, T.C., Tharammal, T., Meyer, V., Lückge, A., Paul, A., Schefuß, E., 2014. Evolution of the Indian Summer Monsoon and terrestrial vegetation in the Bengal region during the past 18 ka. Quat. Sci. Rev. 102, 133–148.
Contreras-Rosales, L.A., Jennerjahn, T., Steinke, S., Mohtadi, M., Schefuß, E., 2019. Holocene changes in biome size and tropical cyclone activity around the Northern South China Sea. Quat. Sci. Rev. 215, 45–63.
Cui, L., Hu, J., Wang, X., 2018. Spatiotemporal evolution of C_3/C_4 vegetation and its controlling factors in southern China since the last glacial maximum. Sci. China Earth Sci. 62, 1256–1268. https://doi.org/10.1007/s11430-018-9225-9.
Dai, L., Weng, C., 2015. Marine palynological record for tropical climate variations since the late Last Glacial Maximum in the northern South China Sea. Deep Sea Res. II 122, 153–162.
Dai, L., Weng, C., Mao, L., 2015. Patterns of vegetation and climate change in the northern South China Sea during the last glaciation inferred from marine palynological records. Palaeogeogr. Palaeoclimatol. Palaeoecol. 440, 249–258.
Diefendorf, A.F., Freimuth, E.J., 2017. Extracting the most from terrestrial plant-derived n-alkyl lipids and their carbon isotopes from the sedimentary record: a review. Org. Geochem. 103, 1–21.
Eggleston, S., Schmitt, J., Bereiter, B., Schneider, R., Fischer, H., 2016. Evolution of the stable carbon isotope composition of atmospheric CO_2 over the last glacial cycle. Paleoceanography 31, 434–452.
Eglinton, G., Hamilton, R.J., 1967. Leaf epicuticular waxes. Science 156, 1322–1335.
Ehleringer, J.R., 2005. The influence of atmospheric CO_2, temperature, and water on the abundance of C_3/C_4 taxa. In: Ehleringer, J.R., Cerling, T.E., Dearing, M.D. (Eds.), A History of Atmospheric CO_2 and its Effect on Plants, Animals, and Ecosystems. Springer Verlag, NY, pp. 214–231.
Ehleringer, J.R., Cerling, T.E., Helliker, B.R., 1997. C_4 photosynthesis, atmospheric CO2, and climate. Oecologia 112, 285–299.
Farquhar, G.D., Ehleringer, J.R., Hubick, K.T., 1989. Carbon isotope discrimination and photosynthesis. Annu. Rev. Plant Biol. 40, 503–537.
González, C., Dupont, L.M., 2009. Tropical salt marsh succession as sea-level indicator during Heinrich events. Quat. Sci. Rev. 28, 939–946.
Grant, K.M., Rohling, E.J., Ramsey, C.B., Cheng, H., Edwards, R.L., Florindo, F., Heslop, D., Marra, F., Roberts, A.P., Tamisiea, M.E., Williams, F.H., 2014. Sea-level variability over five glacial cycles. Nat. Commun. 5, 5076. https://doi.org/10.1038/ncomms6076.
He, J., Jia, G., Li, L., Wang, P., 2017. Differential timing of C_4 plant decline and grassland retreat during the penultimate deglaciation. Global Planet. Change 156, 26–33.
He, J., Zhao, M.X., Li, L., Wang, P.X., Ge, H.M., 2008. Sea surface temperature and terrestrial biomarker records of the last 260 ka of core MD05-2904 from the northern South China Sea. Chin. Sci. Bull. 53, 2376–2384.
Horton, B.P., Shennan, I., Bradley, S.L., Cahill, N., Kirwan, M., Kopp, R.E., Shaw, T.A., 2018. Predicting marsh vulnerability to sea-level rise using Holocene relative sea-level data. Nat. Commun. 9 https://doi.org/10.1038/s41467-018-05080-0.
Huang, E., Chen, Y., Schefuß, E., Steinke, S., Liu, J., Tian, J., Martínez-Méndez, G., Mohtadi, M., 2018. Precession and glacial-cycle controls of monsoon precipitation isotope changes over East Asia during the Pleistocene. Earth Planet Sci. Lett. 494, 1–11.
Huang, Y., Street-Perrott, F.A., Metcalfe, S.E., Brenner, M., Moreland, M., Freeman, K.H., 2001. Climate change as the dominant control on glacial-interglacial variations in C_3 and C_4 plant abundance. Science 293, 1647–1651.
International Atomic Energy Agency, 2013. Global Network of Isotopes in Precipitation (GNIP): the GNIP database. http://www-naweb.iaea.org/napc/ih/IHS_resources_gnip.html.
Jackson, J.F., 1978. Seasonality of flowering and leaf-fall in a Brazilian subtropical lower montane moist forest. Biotropica 10, 38–42.
Jia, G., Bai, Y., Yang, X., Xie, L., Wei, G., Ouyang, T., Chu, G., Liu, Z., Peng, P.a., 2015. Biogeochemical evidence of Holocene East Asian summer and winter monsoon variability from a tropical maar lake in southern China. Quat. Sci. Rev. 111, 51–61.
Jiang, W., Wu, H., Li, Q., Lin, Y., Yu, Y., 2019. Spatiotemporal changes in C_4 plant abundance in China since the Last Glacial Maximum and their driving factors. Palaeogeogr. Palaeoclimatol. Palaeoecol. 518, 10–21.
Lee, C.-Y., Liew, P.-M., 2010. Late Quaternary vegetation and climate changes inferred from a pollen record of Dongyuan Lake in southern Taiwan. Palaeogeogr. Palaeoclimatol. Palaeoecol. 287, 58–66.
Li, J., 1991. The environmental effects of the uplift of the Qinghai-Xizang Plateau. Quat. Sci. Rev. 10, 479–483.
Li, J., Fang, S., 1996. Studies on the uplift and environmental changes of the Qinghai-Xizang Plateau. Chin. Sci. Bull. 41, 316–322.
Liew, P.-M., Huang, S.-Y., Kuo, C.-M., 2006. Pollen stratigraphy, vegetation and environment of the last glacial and Holocene - a record from Toushe Basin, central Taiwan. Quat. Int. 147, 16–33.
Lisiecki, L.E., Raymo, M.E., 2005. A Pliocene-Pleistocene stack of 57 globally distributed benthic δ^{18}O records. Paleoceanography 20. https://doi.org/10.1029/2004PA001071. PA 1003.
Liu, J., Steinke, S., Vogt, C., Mohtadi, M., De Pol-Holz, R., Hebbeln, D., 2017. Temporal and spatial patterns of sediment deposition in the northern South China Sea over the last 50,000 years. Palaeogeogr. Palaeoclimatol. Palaeoecol. 465, 212–224.
Liu, J., Wang, W., 2004. A discussion on the vegetation types during LGM time in South China. Quat. Sci. 24, 213–216 (In Chinese with English abstract).
Liu, S., Jiang, D., Lang, X., 2018. A multi-model analysis of moisture changes during the last glacial maximum. Quat. Sci. Rev. 191, 363–377.
Liu, Z., Huang, W., Li, J., Wang, P., Wang, R., Yu, K., Zhao, J., 2009. Chapter 4: sedimentology. In: Wang, P., Li, Q. (Eds.), The South China Sea: Paleoceanography and Sedimentology. Springer, pp. 171–295.
Liu, Z., Wen, X., Brady, E.C., Otto-Bliesner, B., Yu, G., Lu, H., Cheng, H., Wang, Y., Zheng, W., Ding, Y., Edwards, R.L., Cheng, J., Liu, W., Yang, H., 2014. Chinese cave records and the East Asia summer monsoon. Quat. Sci. Rev. 83, 115–128.
Liu, Z., Zhao, Y., Colin, C., Stattegger, K., Wiesner, M.G., Huh, C.-A., Zhang, Y., Li, X., Sompongchaiyakul, P., You, C.-F., 2016. Source-to-sink transport processes of fluvial sediments in the South China Sea. Earth Sci. Rev. 153, 238–273.
Luo, C.X., Chen, M.H., Xiang, R., Liu, J.G., Zhang, L.L., Lu, J., Yang, M.X., 2014. Characteristics of modern pollen distribution in surface sediment samples for the northern South China Sea from three transects. Quat. Int. 286, 148–158.
Luo, Y., Sun, X., Jian, Z., 2005. Environmental change during the penultimate glacial cycle: a high-resolution pollen record from ODP Site 1144, South China Sea. Mar. Micropaleontol. 54, 107–123.
Milliman, J.D., Farnsworth, K.L., 2011. River Discharge to the Coastal Ocean: a Global Synthesis. Cambridge University Press, Cambridge, p. 384.
Mohtadi, M., Bergenthal, M., Contreras, A., Dang, H., Dubmann, R., Freudenthal, T., Ge, H., Iliev, M., Kaszemeik, K., Keil, H., Klann, M., Klein, T., Li, X., Liang, D., Luckge, A., Munz, P., Palamenghi, L., Rehage, R., Reich, R., Reuter, M., Rosiak, U., Schmidt, W., Steinke, S., Weiner, A., 2012. Report and Preliminary Results of RV Sonne Cruise SO 221, INVERS. Hongkong-Hongkong, 17.05.2012 - 07.06.2012, Berichte. Fachbereich Geowissenschaften, Universität Bremen, p. 168. http://nbn-resolving.de/urn:nbn:de:gbv:46-00102735-15.
Ni, J., Yu, G., Harrison, S.P., Prentice, I.C., 2010. Palaeovegetation in China during the late Quaternary: Biome reconstructions based on a global scheme of plant functional types. Palaeogeography, Palaeoclimatology, Palaeoecology 289, 44–61.
Pelejero, C., 2003. Terrigenous *n*-alkane input in the South China Sea: high-resolution records and surface sediments. Chem. Geol. 200, 89–103.
Peng, T.-R., Wang, C.-H., Huang, C.-C., Fei, L.-Y., Chen, C.-T.A., Hwong, J.-L., 2010. Stable isotopic characteristic of Taiwan's precipitation: a case study of western Pacific monsoon region. Earth Planet Sci. Lett. 89, 357–366.
Portmann, F.T., Siebert, S., Döll, P., 2010. MIRCA2000-Global monthly irrigated and rainfed crop areas around the year 2000: a new high-resolution data set for agricultural and hydrological modeling. Global Biogeochem. Cycles 24, GB1011. https://doi.org/10.1029/2008GB003435.
Sage, R.F., 2004. The evolution of C_4 photosynthesis. New Phytol. 161, 341–370.
Schefuß, E., Kuhlmann, H., Mollenhauer, G., Prange, M., Pätzold, J., 2011. Forcing of wet phases in southeast Africa over the past 17,000 years. Nature 480, 509–512.
Schefuß, E., Schouten, S., Jansen, J.F., Damste, J.S.S., 2003. African vegetation controlled by tropical sea surface temperatures in the mid-Pleistocene period. Nature 422, 418–421.
Schefuß, E., Schouten, S., Schneider, R.R., 2005. Climatic controls on central African hydrology during the past 20,000 years. Nature 437, 1003–1006.
Schmitt, J., Schneider, R., Elsig, J., Leuenberger, D., Lourantou, A., Chappellaz, J., Köhler, P., Joos, F., Stocker, T.F., Leuenberger, M., 2012. Carbon isotope constraints on the deglacial CO_2 rise from ice cores. Science 336, 711–714.
Sheng, M., Wang, X., Zhang, S., Chu, G., Su, Y., Yang, Z., 2017. A 20,000-year high-resolution pollen record from Huguangyan Maar Lake in tropical-subtropical South China. Palaeogeogr. Palaeoclimatol. Palaeoecol. 472, 83–92.
Sun, X., Li, X., 1999. A pollen record of the last 37 ka in deep sea core 17940 from the northern slope of the South China Sea. Mar. Geol. 156, 227–244.
Sun, X., Li, X., Luo, Y., Chen, X., 2000. The vegetation and climate at the last glaciation on the emerged continental shelf of the South China Sea. Palaeogeogr. Palaeoclimatol. Palaeoecol. 160, 301–316.
Sun, X., Luo, Y., Huang, F., Tian, J., Wang, P., 2003. deep-sea pollen from the south China sea: pleistocene indicators of east Asian monsoon. Mar. Geol. 201, 97–118.
Tabor, C.R., Otto-Bliesner, B.L., Brady, E.C., Nusbaumer, J., Zhu, J., Erb, M.P., Wong, T.E., Liu, Z., Noone, D., 2018. Interpreting precession-driven δ^{18}O variability in the South Asian monsoon region. J. Geophys. Res. Atmos. 123, 5927–5946.
Takeda, T., 1985. Studies on the ecology and geographical distribution of C_3 and C_4 grasses III. Geographical distribution of C_3 and C_4 grasses in relation to climatic

conditions in India subcontinent. Japan. Crop Sci. 54, 365–372 (In Japanese with English abstract).
Tharammal, T., Paul, A., Merkel, U., Noone, D., 2013. Influence of last glacial maximum boundary conditions on the global water isotope distribution in an atmospheric general circulation model. Clim. Past 9, 789–809.
Thomas, E.K., Clemens, S.C., Prell, W.L., Herbert, T.D., Huang, Y., Liu, Z., Sinninghe Damste, J.S., Sun, Y., Wen, X., 2014. Temperature and leaf wax δ^2H records demonstrate seasonal and regional controls on Asian monsoon proxies. Geology 42, 1075–1078.
Wang, P., Min, Q., Bain, Y., Cheng, X., 1981. Strata of Quaternary transgressions in East China: a preliminary study. Acta Geol. Sin. 1, 1–13 (In Chinese with English abstract).
Wang, P., Min, Q., Bain, Y., Cheng, X., 1985. On micropaleontology and stratigraphy of Quaternary marine transgressions in East China. In: Wang, P. (Ed.), Marine Micropaleontology of China. China Ocean Press/Springer, Beijing/Berlin, pp. 265–284.
Wang, P.X., Wang, B., Cheng, H., Fasullo, J., Guo, Z., Kiefer, T., Liu, Z., 2014. The global monsoon across time scales: coherent variability of regional monsoons. Clim. Past 10, 1–46.
Wang, R., Ma, L., 2016. Climate-driven C_4 plant distributions in China: divergence in C_4 taxa. Sci. Rep. 6, 27977. https://doi.org/10.1038/srep27977.
Wang, S., Lu, H., Han, J., Chu, G., Liu, J., Negendank, J.F., 2012. Palaeovegetation and palaeoclimate in low-latitude southern China during the last glacial maximum. Quat. Int. 248, 79–85.
Xiao, J., Shang, Z., Shu, Q., Yin, J., Wu, X., 2018. The vegetation feature and palaeoenvironment significance in the mountainous interior of southern China from the Last Glacial Maximum. Sci. China Earth Sci. 61, 71–81.
Xue, J., Zhong, W., Cao, J., 2014. Changes in C_3 and C_4 plant abundances reflect climate changes from 41,000 to 10,000 yr ago in northern Leizhou Peninsula, South China. Palaeogeogr. Palaeoclimatol. Palaeoecol. 396, 173–182.
Xue, J., Zhong, W., Xie, L., Unkel, I., 2015. Vegetation responses to the last glacial and early Holocene environmental changes in the northern Leizhou Peninsula, south China. Quat. Res. 84, 223–231.
Yang, S., Ding, Z., Li, Y., Wang, X., Jiang, W., Huang, X., 2015. Warming-induced northwestward migration of the East Asian monsoon rain belt from the Last Glacial Maximum to the mid-Holocene. Proc. Natl. Acad. Sci. Unit. States Am. 112, 13178–13183.
Yin, L., Li, M., 1997. Ecology of C_4 plants in China I. C_4 plants distribution in China and their relation with regional climatic conditions. Acta Ecol. Sin. 17, 350–363 (In Chinese with English abstract).
Yu, S., Zheng, Z., Chen, F., Jing, X., Kershaw, P., Moss, P., Peng, X., Zhang, X., Chen, C., Zhou, Y., Huang, K., Gan, H., 2017. A last glacial and deglacial pollen record from the northern South China Sea: new insight into coastal-shelf paleoenvironment. Quat. Sci. Rev. 157, 114–128.
Zheng, Z., Huang, K., Deng, Y., Cao, L., Yu, S., Suc, J.-P., Berne, S., Guichard, F., 2013. A ~200 ka pollen record from Okinawa Trough: paleoenvironment reconstruction of glacial-interglacial cycles. Sci. China Earth Sci. 56, 1731–1747.
Zheng, Z., Lei, Z.-Q., 1999. A 400,000 year record of vegetational and climatic changes from a volcanic basin, Leizhou Peninsula, southern China. Palaeogeogr. Palaeoclimatol. Palaeoecol. 145, 339–362.
Zhou, B., Zheng, H., Yang, W., Taylor, D., Lu, Y., Wei, G., Li, L., Wang, H., 2012. Climate and vegetation variations since the LGM recorded by biomarkers from a sediment core in the northern South China Sea. J. Quat. Sci. 27, 948–955.